A Detector for Muon Tomography: Data Acquisition and Preliminary Results

Eric T. Wright

May 2007

Abstract

I describe the general design of the prototype particle detector constructed by the Maya Muon Tomography Group and how it can be used to effectively "x-ray" building and ground structure in a location of interest using cosmic-ray muons. I give detailed descriptions of the high level data acquisition and tracking systems, which are responsible for reconstructing muon trajectories from raw data. In addition, I present the first images obtained from the detector. These images show the basic features of several University of Texas buildings in the vicinity of the Engineering Science Building and demonstrate the feasibility of muon tomographic imaging with our detector.

Contents

1 Introduction

The research of the Maya Muon Tomography Group focuses on:

1. Developing a detector to determine trajectories of cosmic-ray muons[1].

2. Estimating muon flux over a region of interest using a large sample of recorded trajectories

3. Constructing an image of the region interest using the estimated muon flux

Since the most basic principle behind our detector's operation is the constant bombardment of Earth by cosmic radiation, I begin with some history and basic technical background of cosmic rays.

1.1 Cosmic Rays

Cosmic rays are charged particles of unknown extraterrestial origin that continually strike the earth. They were first discovered by Victor Hess in 1912 [4]. Hess observed ion production in an electrometer[2]carried on a manned balloon. He found that ion production doubled as the balloon rose from 1000 to 4000 meters above the ground, indicating the presence of some kind of ionizing radiation penetrating the atmosphere. Cosmic ray research has been an active field ever since; there are many ongoing efforts to measure the composition, flux, and energy spectrum of cosmic rays. Experiments have determined that about 80 percent of incoming cosmic rays are protons and another 14 percent are alpha particles [2]. The incoming nucleons, referred to as primaries, generally interact in the atmosphere to produce a shower of secondary particles. The intensity of incident primaries at the top of the atmosphere is given approximately by

$$I_N(E) \approx 1.8E^{-2.7} \frac{nucleons}{cm^2\ sr\ s\ GeV}, \tag{1}$$

where E is the energy per nucleon. This form is valid for energies above a few GeV up to about 100 TeV. Some primaries have much higher energy; ongoing research collaborations seek to determine the energy spectrum for

[1] Muons are charged, elementary particles belonging to the lepton family, which also consists of the electron, the tau and neutrinos. A muon is roughly 200 times more massive than an electron.

[2] A device used to measure electric charge

these “ultra high energy” cosmic rays. The AGASA detector in Japan and the High Resolution Fly’s Eye in Utah estimated the energy of high energy primaries by studying air showers generated by cosmic ray interactions within the atmosphere. Both claimed to observe cosmic rays with energies above 5×10^{19} ev - much higher than any energies attainable in a particle accelerator.

The production of seconardy muons from cosmic ray interactions is of particular interest to our research. Muons (μ^+/μ^-) are created in a cosmic ray shower from the decay of hadronic secondary particles; the largest producers being charged pions and kaons[3]. Pions (π) and kaons (K) are produced as nucleons interact with nitrogen and oxygen nuclei in the atmosphere. Figure 1 shows a schematic of a typical cosmic-ray shower, with charged meson production feeding the creation of muons. Muons are the

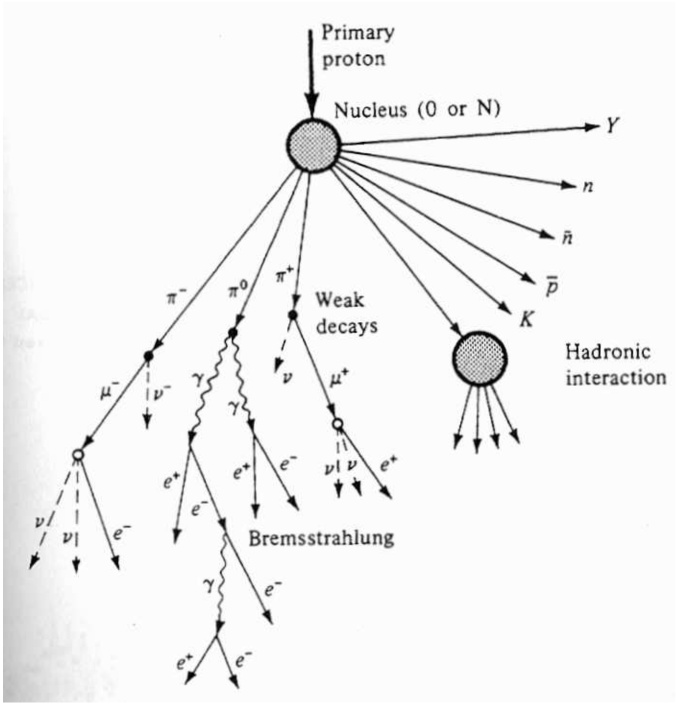

Figure 1: Cosmic ray shower development [4]

[3] Pions and kaons are composite particles consisting of a quark-antiquark pair. They are more generally classified as mesons.

most prevalent decay products of charged pions and kaons:

$$\pi^+/K^+ \rightarrow \mu^+\nu_\mu, \tag{2}$$

$$\pi^-/K^- \rightarrow \mu^-\bar{\nu_\mu}. \tag{3}$$

Charged pions with energies greater than about 100 GeV can interact with nitrogen and oxygen in the atmosphere, producing additional cascades of secondary particles before decaying [3]. However, lower energy charged pions will most likely undergo weak force decay before they can interact with the atmosphere. This is due to the fact that charged pions have a mean proper lifetime of 26 ns, which implies a mean free path before decay of about 55 meters for a 1 GeV charged pion. The pion travels through a very small fraction of the atmosphere; thus, interactions are unlikely.

Figure 2 shows the flux of various components of cosmic ray showers as a function of atmospheric depth. Lower energy charged pions tend to decay to muons/neutrinos around 10 to 15 km above the earth. Muons, having a mean proper lifetime of 2200 ns, tend to penetrate deep into the atmosphere; those with energies above 5 GeV or so can reach far underground before decaying. The implications of figure 2 are clear: muons will be the most readily measurable products of cosmic rays near the surface of the earth.

Muons continually strike the surface of the earth; a 1 cm^2 horizontal muon detector at sea level would see one muon per minute on average. Figure 3 shows the energy spectrum of sea level muons at two different zenith angles.[4] At large zenith angles, low energy muons decay before reaching the ground and high energy pions decay before they can interact with the atmosphere [2]. The result is a higher average muon energy at large zenith angles.

The overall angular distribution of sea level muons is proportional to $cos^2\theta$, where θ is the zenith angle. This implies that more total muons are detected per unit surface area at low zenith angles, while figure 3 shows that more high energy muons are detected per unit surface area at large zenith angles. This property of the muon sea level spectrum is particularly relevant to our detector, as I will explain later.

1.2 Principles of Muon Tomography

Muon Tomography was developed by L.W. Alvarez, [5] et al, in the 1960s in order to study the inside of the Chephren's Second Pyramid in Egypt.

[4] Zenith angle is the angle measured from the vertical axis; that is, 0° zenith is straight up, 90° zenith is horizontal.

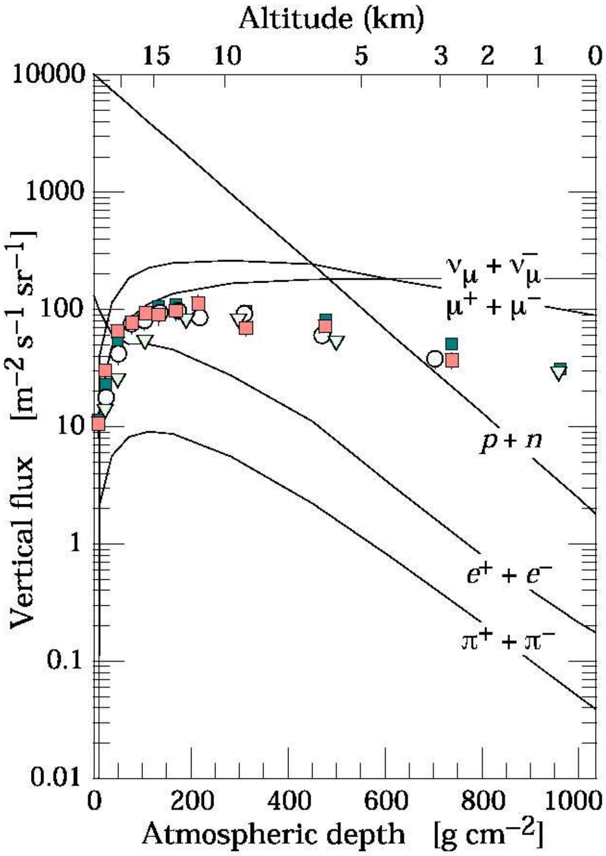

Figure 2: Vertical fluxes of cosmic rays in the atmosphere with energy greater than 1 GeV. The points show measurements of negative muons with energy greater than 1 GeV. [2]

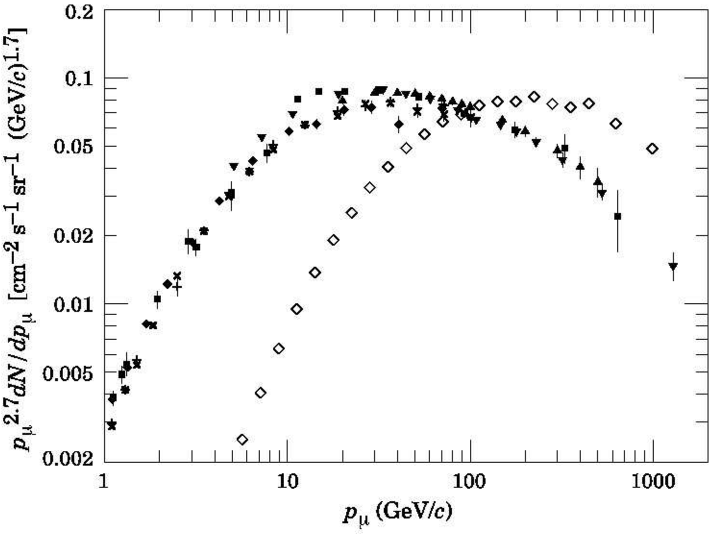

Figure 3: Spectrum of muons measured from sea level. The dark points are at 0° zenith, while the hollow points are at 75° zenith. [2]

Alvarez used the natural flux of cosmic ray muons to produce a density scan of the pyramid. His goal was to find evidence for undiscovered tunnels or chambers within the pyramid. He set up particle detectors inside a cavity underneath the base of the pyramid to measure muon flux as a function of zenith angle. By comparing his measurements of muon flux under the pyramid against the natural background of muons, Alvarez was able to distinguish the meter-scale limestone caps on the outside of the pyramid. He did not find evidence for hidden chambers or tunnels, but he did show the validity of muon tomography as a way to probe the bulk structure of matter.

The principle behind the method is simple: regions of low density material will allow more muons to pass through and reach the detector than regions of high density material. An image of a location of interest is constructed as follows:

- Muon flux is measured at a variety of angles and locations over the target volume

- Differences in flux between particular angles and directions are used to produce a 3D image of the target volume using standard techniques of computer-assisted tomography

A major source of uncertainty in muon tomography is the assumption that the muon trajectory is constant, that is, that the direction determined at the detector is a valid estimate of the direction from which the muon ultimately came. In reality, muons ionize solid material as they pass through, losing energy and possibly scattering in the process. This process is known as multiple-Coulomb scattering. Figure 4 illustrates the uncertainty in a muon track due to scattering. The probability of scattering decreases as the muon energy increases. Therefore, the solution for minimizing tracking errors associated with scattering is to only consider muons with an energy large to enough to have a low probability of scattering through the material of interest. Muons lose approximately 2.2 MeV for every gm/cm^2 of matter they travel through. Using this basic energy loss formula, it can be shown [1] that for a material with density $\rho = 2.3gm/cm^3$, the cutoff muon energy should be around 2.5 GeV. This insures that the muon spectrum is "hardened" at the detector. Alvarez accomplished this by surrounding his detector with blocks of iron. This way, lower energy muons were absorbed into the iron and not considered in the flux measurements.

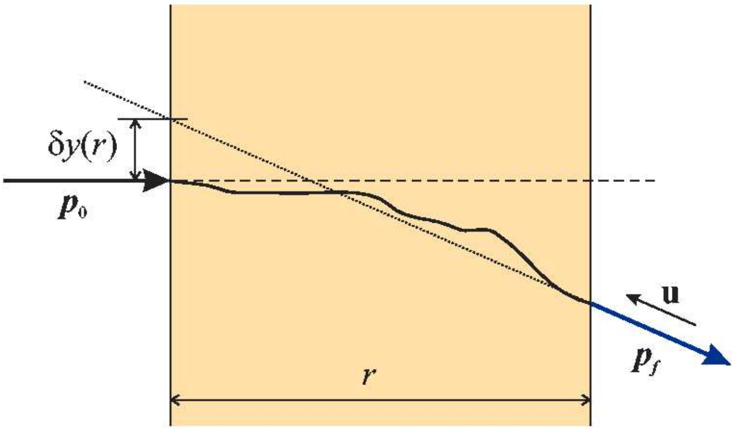

Figure 4: Schematic of a muon undergoing multiple-Coulomb scattering in a dense medium. The detected muon momentum is p_f, while the muon momentum prior to entering the medium is p_0. [1]

In the following section, I will go over the design of our detector and how it accomplishes the tasks of tomography.

2 Detector Design

Our detector for muon tomography is a cylinder with an axial length of 4.22 meters and a mean radius of .8 meters. It is meant to have a vertical orientation with respect to the target volume of interest, that is, it stands on one of its ends like a soup can near the outer edge of the target. The detector measures particle trajectories through its cylindrical face, thus it has a blind region in the shape of a cone about its axis. Figure 5 shows a hypothetical target volume with two such detectors on opposite ends of the volume. An advantage of the cylindrical geometry is that it hardens the spectrum of incident muons by rejecting tracks from low zenith angles.

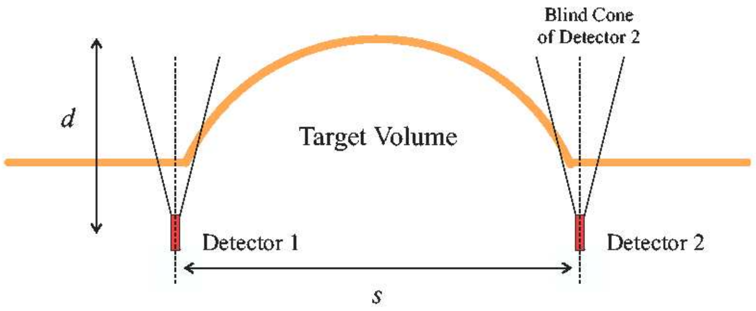

Figure 5: Schematic diagram of the arrangement of two detectors. [1]

The basic unit of our tracking system is a polystyrene scintillator strip running the length of the detector with an embedded wavelength-shifting (WLS) optical fiber. Each strip is approximately 31 mm wide and 10 mm thick with 1.2 mm diameter optical fiber mounted in a groove within the top face of the strip. Figure 6 shows a schematic of a single scintillator strip from two viewpoints. The scintillation material emits light as ionizing radiation passes through it. The optical fiber absorbs some of this light and re-emits it at a slightly different wavelength. The fiber transports this light, with some attenuation, in both directions to the ends of the detector. Photomultiplier tubes (PMTs) housed at both ends of the detector convert the light into an electronic signal for further processing by our data acquisition system. The properties of these strips and WLS fibers are well understood by the MINOS group; much work has gone into studying the absortion spectrum and attenuation of the WLS fibers through monte carlo simulation and experiment [6].

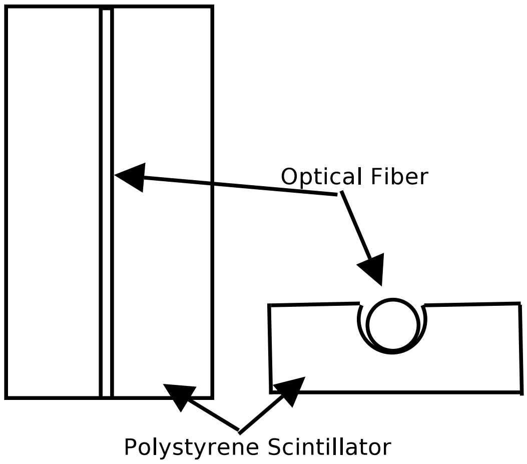

Figure 6: A polystrene scintillator strip with embedded optical fiber. The view on the left is looking down on the outside face of the strip. The view on the right is at eye level looking down the length of the strip

The scintillator strips in each layer are mounted side-by-side, completely covering the outside face of the detector. The inside and outside layer of scintillator strips are wrapped around the detector in helical patterns; the pitch angles[5]are $-30.30°$ and $30.07°$ for the inside and outside layers, respectively. The middle layer of strips is straight with respect to the detector length. There are a total of 441 strips mounted on the detector with 136 strips in the inside layer, 163 strips in the middle layer, and 142 strips in the outside layer. Figure 7 shows a schematic of this layout, with small sections of each strip layer pictured.

The electronics system used to read out the light pulses generated by the scintillation strips consists of Hamamatsu M64 multianode PMTs, front-end boards (FEBs), and a National Instruments CompactRIO real-time controller. Each end of the detector has its own set of 7 PMTs with 64 channels each, 14 FEBs with 32 channels each, and 1 RIO box. A single optical fiber uses one channel on a PMT, so each PMT can accomodate a bundle of 64 fibers. Each PMT is connected to two FEBs. An FEB contains circuitry to amplify, shape, and disciminate analog signals from a PMT as well an FPGA for digital processing. The RIO box houses a master clock running at 40 MHz, which it distributes to all the FEBs. The main job of an FEB

[5] Angle measured with respect to the length axis of the detector

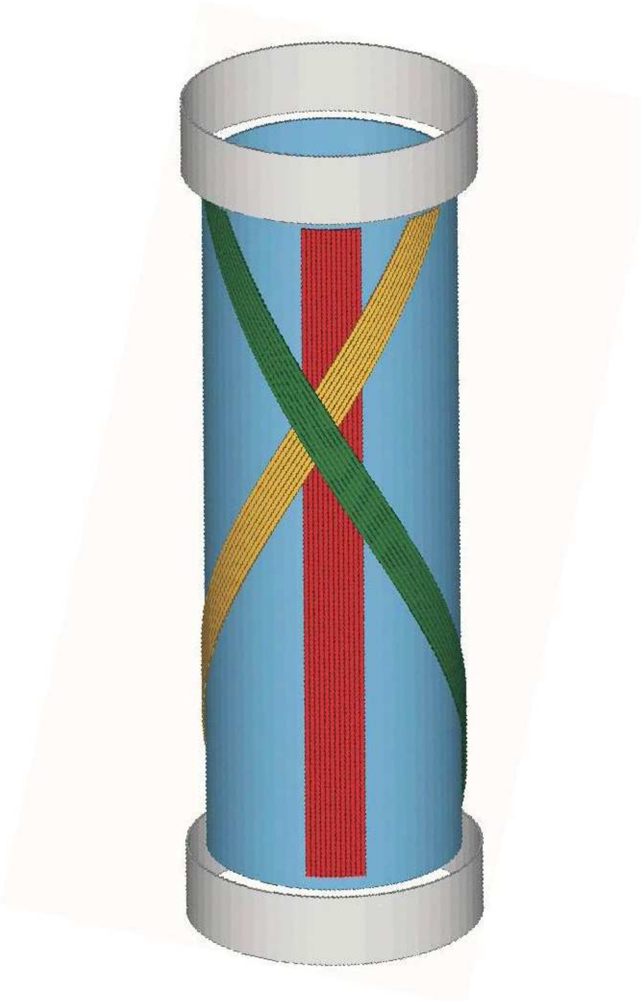

Figure 7: Arrangement of scintillator strips mounted on the detector. PMTs and front-end electronics are mounted in the ringed regions on each end of the detector. [1]

is to discriminate a PMT pulse and add a timestamp to it using the master clock. The RIO box then assembles the data blocks created by the FEBs and sends them to a host computer running National Instruments Labview software. The result of this process is a four byte block for each discriminated PMT pulse; the high 9 bits indicate the unique channel from which the pulse came from (a number between 1 and 448), while the other 23 bits are the timestamp for that pulse. The channel number essentially identifies a single activated scintillator strip. I refer to the overall process described above as the low level data acquisition (DAQ) system. The low level DAQ serves as an interface between the "real" world and the reconstruction software, which uses patterns of activated scintillator strips to calculate muon trajectories.

The layout of the strip layers is designed to maximize strip intersections between layers. For perfectly designed strip layers having complete coverage with no gaps between strips or inactive regions, a particle passing through the detector would go through a strip on each layer as it enters the cylinder and as it exits. Thus, an area where three strips intersect represents a possible entrance or exit point of a muon track. We refer to these intersections as triplets. It is the job of the high level data acquisition software to assemble triplets from the 4 byte hit blocks it receives from the RIO box. In the next section, I describe this process in detail as well as the subsequent track reconstruction process.

3 High Level Data Acquisition

The High Level Data Acquisition (HiDAQ) begins where the RIO box leaves off. The RIO box initiates a data stream of hit blocks which must first be transported to HiDAQ. HiDAQ then filters the data stream, extracts triplets, reconstructs the geometric parameters necessary to describe a trajectory, and stores the resulting trajectory in a meaningful way. I will start with an overview of each one of these processes and then give a description of the HiDAQ software that carries them out.

3.1 Processing the Data Stream

3.1.1 Transportation

All the physically separate parts of the data acquisition system communicate through ethernet connections. In particular, the initial data stream will be sent to HiDAQ over TCP/IP protocol, which ensures that all data is transmitted and received correctly and in order. The first job of HiDAQ is to read the initial stream (one for each end of the detector) from a TCP socket. At the current time, HiDAQ resides on the host computer which controls the RIO box through Labview. However, this is not a requirement; HiDAQ can operate anywhere a TCP/IP connection can be made.

3.1.2 Filtering

The RIO box manufactures data at a rate of roughly 10 MB per minute[6]. Most of this is due to spurious pulses in the optical fibers, electronic noise, and other unknown sources; approximately 85 percent of the original data stream is meaningless for our purpose. In order to extract the potentially useful part of the stream, the filtering segment of HiDAQ looks for strip hits "clumped" together in time. The time difference between two adjacent timestamps is 25 ns, since the clock runs at 40 MHz. Therefore, we would expect all the timestamps on separate strip hits to be within one or two of each other for a muon traveling close to the speed of light. Noise hits tend to come tens to hundreds of timestamps apart, easily separating them from true particle tracks. The requirement to pass the filtering step, then, is a clump of at least six hits all within five timestamps (125 ns) of each other.[7]

Work is currently underway to move the filtering step into the low level DAQ system. This would greatly reduce the load on the transportation system. Another benefit would be increased filtering speed due to using lower level computing procedures.

3.1.3 Triplet Extraction

The next step in the processing is to look for triplets in the clumps of strip hits. First, the channel numbers from the data blocks are translated into their layer/strip numbers using a pre-made map file. Then HiDAQ checks that there are at least two hits present from each layer; if not, it is impossible to form two triplets. If this step is passed, HiDAQ proceeds to triplet finding. This is done quickly by constructing a lookup table of triplets indexed by strip number before HiDAQ begins executing.

The triplet table is built by iterating over all possible intersections of strips in the two helical (stereo) strip layers and determining which axial strips could form a possible triplet with a given stereo intersection. See Figure 8 for a schematic of the geometry. From here on, we define a standard

[6] This is the raw data rate with the current ASD configurations

[7] Some time padding is added into the cut to allow for delays at the FEB level

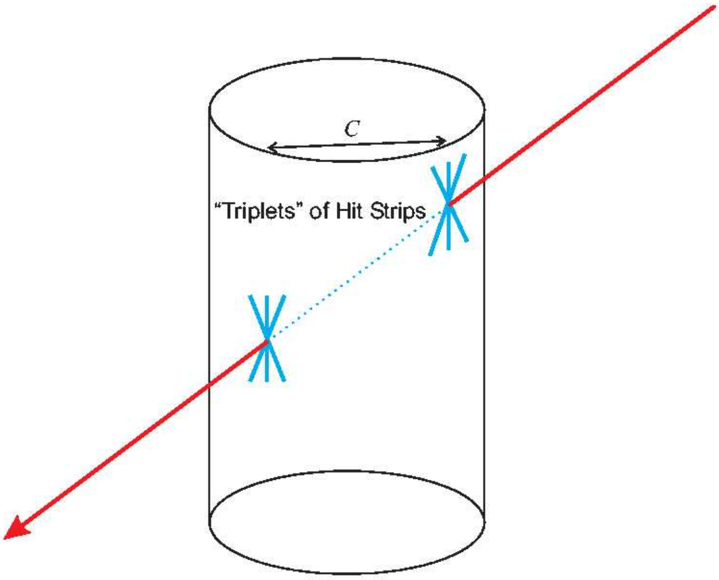

Figure 8: Schematic diagram of a track forming two triplets with chord length of c. [1]

cylindrical coordinate system with the positive z axis pointing along the length of the detector toward the top end and the origin located in the middle of the detector, so that the plane $z = 0$ cuts the detector in half at its midpoint. The axial layer strips usually do not exactly overlap a stereo intersection point; therefore, there are often a few possible triplets for each stereo intersection. We differentiate between the different possibilities by assigning each triplet a χ^2 value according to the formula:

$$\chi^2 = \frac{(\phi_{st} - \phi_0)^2}{w_- + w_+ + w_0}, \tag{4}$$

where ϕ_{st} is the azimuthal angle of the stereo strip intersection, ϕ_0 is the mean azimuthal angle of the axial strip, and the w's are weighing parameters particular to each strip layer which depend on the angular widths of the three strips involved. A χ^2 value of 8 corresponds to the axial strip being one angular strip width away from the stereo intersection. Presently we make a χ^2 cut at 15. This provides a quick way to check if three strips constitute a triplet. We also store the cylindrical coordinates (ϕ, z) for the reconstruction step. The coordinates of each triplet are calculated based on a least squares estimate:

$$\phi = \frac{\phi_{st} - (w_- + w_+)(\phi_{st} - \phi_0)}{w_- + w_+ + w_0}, \tag{5}$$

$$\frac{z}{L} = \frac{\Phi}{\Omega_+ - \Omega_-} - \frac{1}{2}, \tag{6}$$

where L is the length of the detector, Φ is the azimuthal separation between the stereo strips at the bottom end of the detector, and Ω_+ and Ω_- are the azimuthal ranges[8]covered by the outside and inside helical strip layers, respectively; for our detector, these parameters have values 2.9979 and -3.1133 radians.

HiDAQ iterates over all layer/strip hits, using the triplet table χ^2 values to look for valid triplets. We require that a muon track form two triplets separated by a minimum chord distance, c, as shown in Figure 8. Presently we use a chord cut of $c_{min} = 0.6D$, where D is the diameter of the detector. This results in a minimum azimuthal separation of 1.287 radians between triplets. If at least one pair of triplets is found, HiDAQ iterates over all possbile triplet pairs and eliminates the pairs not satisfying the minimum

[8] This parameter indicates how far in azimuth a strip in a helical layer wraps around the cylinder. A Ω of π would indicate that the top and bottom ends of the strip are separated by 180 degrees in azimuth

azimuthal separation requirement. At the end of the above iteration there are three possibilities which will influence future processing:

1. No suitable triplet pairs were found
2. A single pair of triplets were found
3. More than one suitable pair of triplets were found

If 1 is true, HiDAQ throws out this “time clump” and waits for another one. If 2 is true, then the pair is passed to the track reconstruction step. If 3 is true, then the two triplets with smallest χ^2 sum are passed to the track reconstruction step.

3.1.4 Track Reconstruction

The input to the track reconstruction step (recon) is a set of two triplets satisfying the minimum chord cut. The first thing recon does is estimate the track entrance and exit point (in cylindrical coordinates) from the stored triplet coordinates in the triplet table. The entrance is defined as the triplet with the largest z coordinate.[9] Recon then calculates the signed impact parameter[10], b, and the chord distance, c, according to:

$$b = R_0 \cos\left(\frac{\phi_{en} - \phi_{ex}}{2}\right) \tag{7}$$

$$c = 2R_0\sqrt{1 - \left(\frac{b}{R_0}\right)^2}, \tag{8}$$

where R_0 is the mean radius of the detector and ϕ_{en} and ϕ_{ex} are the azimuthal angles of the entrance and exit points.

A correction to account for the thickness of the strip layers is then applied to the entrance and exit points using the estimated b and c parameters. The simplest form of the correction is [7]:

$$\delta\phi = \frac{2tb}{c}, \tag{9}$$

$$\delta z = \frac{2t(z_{en} - z_{ex})}{c^2} \tag{10}$$

[9] We assume that all valid muon tracks are downward going

[10] The distance of closest approach along the track to the detector axis

where t is the strip thickness. The parameters b and c themselves change when the strip thickness is assumed to be non-zero, so the above equations are not a closed form for the corrected coordinates.[11]. Recon recalculates b and c using the thickness corrected entrance and exit points.

Recon finally calculates the track azimuthal[12]and zenith angles:

$$\phi_{track} = \frac{\phi_{en} + \phi_{ex}}{2} - \frac{\pi}{2} \tag{11}$$

$$\theta_{track} = \tan^{-1}\left(\frac{c}{z_{en} - z_{ex}}\right) \tag{12}$$

Using these angles and the impact parameter, b, it is straightforward to calculate the unit vector in the opposite direction of the track, $\vec{u}$, and the coordinates of the point on the track of closest approach to the z axis, X.

3.1.5 Track Storage

HiDAQ writes the essential reconstruction parameters and raw strip hit information to a binary file for long term storage. Each reconstructed track with its associated raw data is referred to as an event in the binary file. The stored parameters are as follows:

- $\vec{u}$ - the unit vector pointing back along the muon track
- X - the point on the track of closest approach to the detector axis
- b - the signed impact parameter
- χ^2_{track} - the sum of the triplet χ^2 values used in the reconstruction
- The median timestamp of the event
- An array containing layer/strip numbers of all the strips activated in the event as well as a flag to indicate if a particular strip was part of one of the triplets used in the reconstruction.

This level of data storage allows easy access to the reconstruction parameters most important for tomography and saves enough of the raw data for the track to be recalculated if necessary.

[11] The closed form is complicated and not shown here. For the full formulas, see the source code of the reconstruction software

[12] When $\phi_{en} > \phi_{ex}$, a factor of π must be subtracted from the average value of ϕ

3.2 Software

HiDAQ is written mostly in C/C++ with a portion written in the JAVA programming language. The data processing steps all take place in compiled C/C++ code in order to ensure runtimes as fast as possible. JAVA provides the graphical front end to the HiDAQ system as it already contains graphical user interface (GUI) components and is portable between multiple operating systems. JAVA also handles the initial transport of the data stream to the HiDAQ computational routines. This is due to JAVA's transparent implementation of the TCP protocol, which would otherwise be extremely operating system dependent.

The JAVA front end along with the C/C++ reconstruction code will eventually comprise a real-time data processing system. Presently, raw data from the detector is stored and processed at a later date by the reconstruction code.

In this section, I briefly describe the major jobs of the HiDAQ software. I begin with the C/C++ computation package. This part of the software consists of seven C++ and two C source files. The tasks of HiDAQ are split between them. I also review some utility programs for managing/visualizing stored track data.

3.2.1 MuGeometry and MuDetector1Geom

MuGeometry defines the basic geometry data structures needed to describe one of our cylindrical detectors. The core of the geometry data structure is the GeomParam structure which provides storage for all the detector dimensional parameters mentioned in the this paper and arrays to store the mean azimuth angles and angular widths of every scintillator strip. There is one array for each layer of strips, with each array indexed by strip number. The MuGeometry class is an abstract base class which is meant to be a blueprint of our detector type. That is, it contains an empty GeomParam structure which should be filled according to the specifics of one detector. The instantiable implementations of this class inherit from MuGeometry and define its Fill() method, which loads geometry data into its GeomParam structure.

Currently there is only one detector, so there is only one concrete implementation of the geometry: MuDetector1Geom. MuDetector1Geom is essentially a spreadsheet containing all the geometry information for the active prototype detector. The code struction used to define detector geometry is purposefully easily extendable to more detectors; future detectors would be named MuDetector2Geom, MuDetector3Geom, etc. They would all inherit from MuGeometry and have the same basic data structure with different numerical values for the geometric parameters.

MuGeometry also has a number of methods dealing with coordinate system tranformation from lab to detector frame. Every defined detector has a set of euler angles and a position vector relative to the lab origin stored with it, so these transformations are easily handled internally by MuGeometry when they are needed.

Throughout HiDAQ data stream processing, the basic unit of detector geometry is an object of type MuDetectorGeom. Any portion of code needing detector geometry in its calculations will be passed a pointer to one of these objects, giving it access to all of the detector geometry information.

3.2.2 MuRecon

MuRecon contains the set of C++ routines that implement triplet finding and track reconstruction. In order to carry out these tasks, it defines and fills the triplet table mentioned in the previous section.

3.2.3 DAQMap and ChannelLayerStripMap

These are two C files comprising the map which translates low level channel numbers into layer/strip numbers needed by the reconstruction to determine track geometry. ChannelLayerStripMap is essentially a spreadsheet with the raw mappings, which DAQMap defines some routines to easily read the map.

3.2.4 MuData, MuReconData and MuHeadData

MuReconData defines the structure of the binary storage file for reconstructed tracks and MuHeadData defines a data header which is meant to be placed at the beginning of each binary file of tracks. The header stores run specific information such as time/date start of run, detector locations and euler angles.

MuData is an abstract class which defines the basic operations of opening, reading, and writing to a binary storage file. The most important task of MuData is to standarize the file input/output operations carried out in the reconstruction code. This means that a binary file written using MuData writing routines can easily be read out at a later time using MuData reading routines. MuData has a very generic design based on the structure of a DST bank storage system. Thus, it is easily adaptable to storing different types of data as the need arises. MuReconData and MuHeadData are both concrete implementations of MuData.

3.2.5 MuRawProcessor

MuRawProcessor is the overseer of the entire data stream processing task. It implements the timestamp filter (although this may be moved to the low level DAQ process soon), sends the resulting clumps of hit blocks to reconstruction routines, and then writes the reconstructed track (if it exists) to the binary storage file.

3.2.6 RawProcess

Raw Process is an executable program that implements a MuRawProcessor, thus it carries out complete track reconstruction from raw data. Its input is a binary file of raw detector hit blocks and it outputs a binary track storage file.

3.2.7 ReconDataDump

ReconDataDump is an executable program that dumps the contents of a binary storage file into an ascii text file. This is extremely useful when one needs to actually see the track calculations.

3.2.8 ReconDataToTree

ReconDataToTree is an executable program that converts binary track storage files into ROOT trees. This is useful for large scale data analysis and histogramming.

3.2.9 JAVA Strip Display

The JAVA display is the graphical front end to HiDAQ. It consists of a realtime display which creates visual representations of track reconstruction. The display has a 3D Track Display, which uses reconstructed track geometry to overlay a track onto a graphical representation of the detector. The strips hit in the event "light" up on detector cylinder in the display. The detector may be rotated around any axis for easier viewing. Track Display is meant to provide a "sanity check" service for the real time reconstruction - if the displayed track doesn't at all fit with the pattern of lit strips, something is clearly going wrong. The other component of the display is a 2D Strip display which shows the strips hit in each layer on a plane surface meant to represent the cylindrical face of the detector "rolled" out flat. Figure 9 shows a screenshot of the display for a typical event.

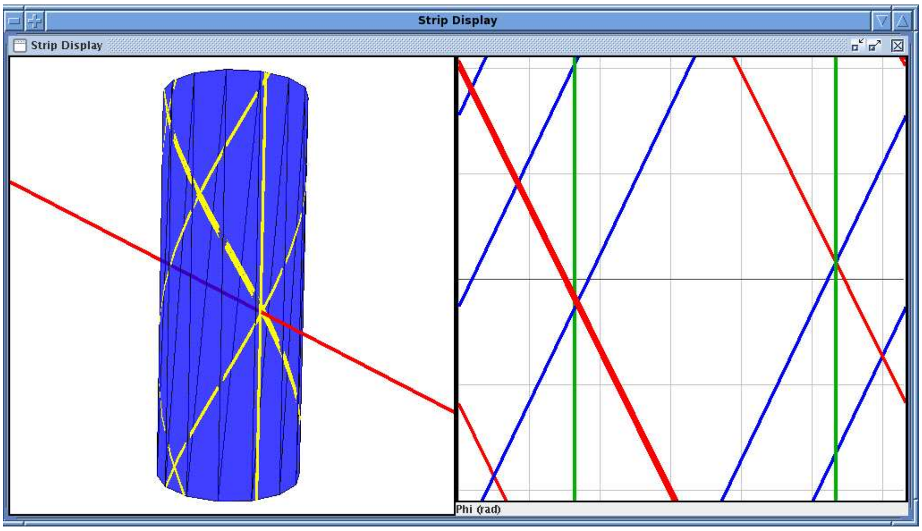

Figure 9: Screenshot of the JAVA graphical frontend to HiDAQ. The panel on left is the 3D Track Display, the panel on the right is the 2D strip display

4 Preliminary Results: First Image

In March 2007 we started collecting muon tracks with the prototype muon detector with the intention of observing structure in the University of Texas buildings surrounding our lab in the Engineering Science Building (ENS). We can see the definite markings of many structures in our vicinity with only ten minutes worth of data. The most obvious object we see is the tower of the ENS building, which lies directly to the south of our detector. We are confident that we are also seeing the muon shadows of the top of RLM to our west and the Cockrell Engineering Building to our north.

We presently visualize our muon flux by constructing a two dimensional histogram of (ϕ, $\cot\theta$) over all collected muon tracks, where ϕ and θ are the azimuthal and zenith angles of a track. This amounts to a projection onto a cylinder of unit radius and infinite height concentric with our detector. The (ϕ, $\cot\theta$) histogram gives us a good qualitative sense about how the muon

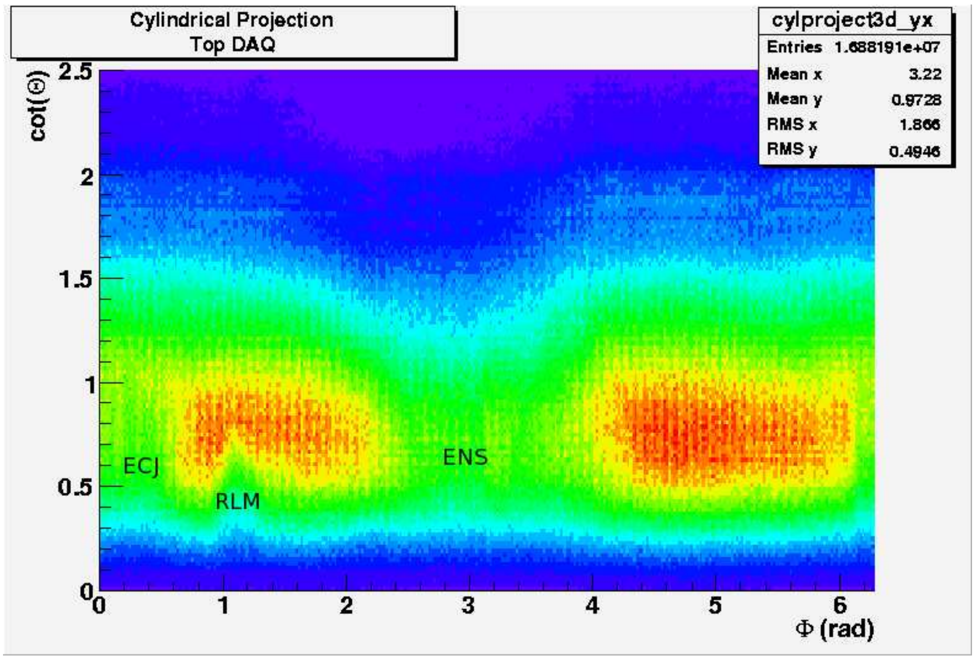

Figure 10: (ϕ, $\cot\theta$) histogram for three hours of data from the top end of the detector. There are 320 bins in ϕ and 125 bins in $\cot\theta$. The muon hit intensity increases with the brightness in the bin color; blue and purple colors indicate less relative tracks per bin, orange and red indicate relatively more tracks per bin. The text indicates approximate locations of nearby University of Texas buildings.

flux varies with a given direction from the detector. Figure 10 shows one such histogram from a three hour data run with the top end of the detector. The zero degree azimuthal reference angle of our detector corresponds roughly to the north direction. The histogram shows a large shadow between 2.5 and 4 radians, which corresponds to the area south of us where the ENS tower is. An area of higher flux from 4 to 6 radians, corresponding to an area to our northeast where there are no buildings, is essentially a measurement of the background muon flux.

5 Conclusion

It is clear that our detector can see the general features of structures around it using muon tomography. In the near future, we expect to study the imaging resolution of our detector and, in the process, develop more sophisticated imaging techniques. This will likely involve collaboration with experts in the field of computerized tomography.

As our imaging capabilities increase, the data acquisition process will have to be fine tuned to achieve the best resolution possible. There are a number of areas where we can improve the existing system:

1. Synchronization of the master clocks in the two RIO boxes on the top and bottom ends of the detector. Currently, we lose tracks due to optical fiber attenuation that we could otherwise reconstruct if we could use one end of the detector to compensate for the other.

2. Replace the portions or all of the Labview DAQ software with custom built low-level modules in VHDL.[13]This would provide much more control over the low level DAQ and increase the efficiency of the data flow and clock cycles.

3. Move portions of the reconstruction into the low level DAQ. Work is already underway to move the filtering step. This will reduce the size of the data stream by roughly 85 percent entering the reconstruction step.

4. Implementing a cherenkov radiation threshold system in order to reject muons with incident energies below 2.5 GeV.

Of all the improvements listed above, the cherenkov threshold would be the most difficult to achieve. Nevertheless, it would be a very important addition to the DAQ system.

[13] A Hardware description language used to program FPGAs

References

[1] The Maya Muon Group *A Detector for Muon Tomography* Conceptual Design Report, June 2004.

[2] W.M. Yao, et al. *Particle Data Group Review of Cosmic Rays* Journal of Physics G33, 1. 2006

[3] Perkins, D.H. *Particle Astrophysics* Oxford University Press, 2003.

[4] Frauenfelder, Hans and Henley, Ernest M. *Subatomic Physics* Prentice Hall, 1991.

[5] L.W. Alvarez, et al. *Search for Hidden Chambers in Pyramids using Cosmic Rays* Science **167**, 832-839, 1970.

[6] Loer, Ben *A Geant4 Monte Carlo Simulation of Optical Processes in Scintillator* Bachelor of Science Senior Thesis. May 2006

[7] Schwitters, R.F. *Scintillator Thickness Corrections to Tracking* March 2, 2005.